Nuclear interactions by high-energy cosmic ray nuclei with light nuclei in emulsion

1973 J. Phys. A: Math. Nucl. Gen. 6 1974

(http://iopscience.iop.org/0301-0015/6/12/022)

J. Phys. A: Math., Nucl. Gen., Vol. 6, December 1973. Printed in Great Britain.

Nuclear interactions by high-energy cosmic ray nuclei with light nuclei in emulsion

K Imaeda and P Fleming†

School of Cosmic Physics, Dublin Institute for Advanced Studies, Dublin, Ireland

Received 1 May 1972, in final form 7 August 1973

Abstract. The mechanism of particle production in nucleus–nucleus and nucleus–nucleon collisions produced by high-energy cosmic ray nuclei ($6 \leqslant Z \leqslant 26$) in nuclear emulsion has been studied. Theoretical formulae to estimate the $\ln\tan\theta$ distributions of the individual groups of secondaries have been derived and used for the analysis. It is found that a large proportion of relativistic α particles and protons are produced through the knock-on process as distinct from the fragmentation process. Kaplon's and our formulae for the fragmentation α particles or protons if applied to all the relativistic α particles or protons, would give an underestimation of the primary energy. Mesons are produced more through the isobar than the fireball process in the primary energy interval from 10 to 30 GeV/nucleon, but the meson multiplicity due to the latter process increases faster with increasing energy than for the former process.

1. Introduction

High-energy cosmic ray nuclei contribute not only to extensive air showers through meson production by collisions with air nuclei but also to the high-energy galactic electrons and photons in interstellar space. At present, our knowledge of particle production in nucleus–nucleus collisions at high energy is meagre. Nuclear interactions produced by high-energy heavy cosmic rays in collision with nuclei have been confined mainly to obtaining knowledge concerning the fragmentation process. The difficulty in analysing the particles from nucleus–nucleus collisions has been due to the lack of a reliable method for differentiating the secondaries produced through the different production processes in the interaction. For example, we did not know how to separate theoretically on the $\ln\tan\theta$ plot these various groups of secondaries or how these various groups of secondaries contribute to particle production.

In this paper, based on knowledge of particle production obtained from nucleus–nucleon collisions, theoretical calculations to estimate the $\ln\tan\theta$ distributions, the average $\ln\tan\theta$ values, and the $\ln\tan\theta$ dispersions, are derived for the various groups of secondaries produced in nucleus–nucleus collisions.

By applying these calculations to nucleus–nucleus collisions, an effort is made to separate experimentally the different groups of secondaries produced in the interactions of high-energy cosmic ray primaries ($6 \leqslant Z \leqslant 26$) with the light nuclei (H, C, N, O) in nuclear emulsion.

† Present address: Physics Department, Crawford Municipal Technical Institute, Cork, Ireland.

2. Experimental method

The heavy cosmic ray jets used in this analysis have been found in the Dublin part of the ICEF stack mainly by area scanning. The characteristics of the ICEF stack are mentioned in the ICEF collaboration (1963). Those jets with the number of heavy prongs $N_h \leqslant 8$, and with primary charge $Z_p \geqslant 6$, were selected as being due to collisions with light target nuclei in nuclear emulsion (Rajopodhye and Waddington 1958).

The details of the characteristics of the jets are listed in tables 1 and 2, including the charges and Lorentz factors of the primary nuclei; the multiplicity and charges of the secondary particles: heavy fragments $Z_f > 2$, N_f; α particles, N_α; black tracks, n_b; grey tracks, n_g; and minimum tracks, n_s. Table 1 lists light target nuclei events defined by $1 < N_h \leqslant 8$. Table 2 lists proton or quasi-free proton target events defined by $N_h \leqslant 1$.

Table 1. Nuclear target events ($N_h \leqslant 8$)

Event number	Primary and charge	Lorentz factor	Fragments ($Z_f \geqslant 3$)	α particle	n_s	n_g	n_b
5-25	Na^{11}	64·6	—	2	36	1	1
2-366	Ca^{20}	49·0	—	3	45	1	2
2-37	Al^{13}	45·8	C^6	2	21	4	1
2-37A	C^6	45·8	—	2	7	0	2
2-350	P^{15}	39·7	B^5, Li^3	2	21	4	3
5-21	V^{23}	35·5	—	2	52	3	1
2-155	Mg^{12}	31·0	Li^3	2	48	3	1
11-10	P^{15}	30·2	C^6, Li^3	2	15	1	4
8-12	O^8	29·6	—	1	22	0	2
2-75	Cl^{17}	28·7	O^8	3	12	1	3
2-220	Al^{13}	22·4	Ne^{10}	—	15	3	4
2-269A	Cr^{24}	22·4	K^{19}	—	10	3	3
2-269C	K^{19}	22·4	Al^{13}	2	12	0	4
2-103	Ne^{10}	21·8	—	2	32	4	4
2-349	Cl^{17}	17·2	N^7	1	20	0	3
2-66B	C^6	13·8	—	—	9	1	2
2-254	Mg^{12}	12·9	Li^3	2	21	2	2
5-53	Na^{11}	12·9	—	2	32	1	3
5-107A	Ca^{20}	11·5	S^{16}	—	7	1	1
5-350	A^{18}	10·3	—	1	26	2	0
2-259	F^9	9·1	—	—	16	2	3
2-141	Ne^{10}	4·7	N^7	1	2	1	1

The charges of the primary nuclei (from 6 to 26) were estimated by two independent methods: the fragmentation method and the δ ray count method. In the fragmentation method, we selected six 'proton target' jets which, by the proposed analysis, were confirmed to be due to the disintegration of primary nuclei as no meson production had taken place. We have compared the primary charge determined by the fragmentation method with that determined by the δ ray method. The δ rays were counted on all the primary tracks and on all the fragmentation products of charge $Z > 2$. The charges determined by the δ ray method were normalized for $Z = 6$ to 26 by the fragmentation method.

Table 2. Proton target events ($N_h \leqslant 1$)

Event number	Primary and charge	Lorentz factor	Fragments ($Z_f \geqslant 3$)	α particle	n_s	n_g	n_b
8-22B	F^{9}	145	—	2	11	0	0
5-51	K^{19}	40	—	1	57	0	1
2-127	S^{14}	39	F^{9}	1	12	0	1
2-221	Ne^{10}	34·7	N^{7}	1	8	0	1
8-24	O^{8}	32·4	—	2	9	0	0
2-211	Na^{11}	27·6	B^{5}	1	8	0	0
2-245	P^{15}	27·0	O^{8}	2	7	1	0
2-245A	O^{8}	27·0	—	0	22	0	0
2-171	O^{8}	25·8	—	2	8	1	0
2-355	Si^{14}	25·8	N^{7}	1	8	0	0
5-106	P^{15}	25·8	—	2	32	0	1
2-269D	Al^{13}	22·4	C^{6}	1	10	0	0
2-269E	C^{6}	22·4	—	2	4	0	0
2-351	Cl^{17}	22·4	Ne^{10}	2	15	0	0
2-107	Na^{11}	16·1	Li^{3}	3	2	1	0
2-66	Si^{14}	13·8	N^{7}	2	9	0	0
2-169	O^{8}	13·8	—	2	6	0	0
5-65A	Ca^{20}	13·5	Cl^{17}	1	7	0	0
5-65B	Cl^{17}	13·5	F^{9}, O^{8}	0	5	0	0
2-96	Ne^{10}	13·2	Li^{3}	2	2	0	1
2-102	Na^{11}	12·9	Li^{3}	2	5	1	0
5-165	C^{17}	12·9	F^{9}	1	9	0	0
2-349	N^{7}	12·3	Li^{3}	2	0	1	0
5-107	Fe^{26}	11·5	Ca^{20}	2	3	1	0
2-91	Fe^{26}	8·0	C^{6}, C^{6}	3	11	0	0
2-248	O^{8}	6·9	—	3	2	0	1
2-356	Fe^{26}	6·5	Al^{13}, Li^{3}	3	6	0	0
5-59	Al^{13}	6·3	Li^{3}	2	7	0	0
2-72	Na^{11}	6·2	—	2	7	0	0

The empirical relation between the δ ray density per 100 μm and the charge could be derived and is given by:

$$N_\delta/(100\ \mu\text{m}) = aZ^2(v/c)^{-2} + b, \tag{2.1}$$

where our experimental values of a and b are 0·11 and 0·10 respectively, and $(v/c) \simeq 1$ since we are dealing with relativistic nuclei. The fragmentation method on six events shows that the errors in the estimation of the charge are zero and one for charges $Z < 8$ and $8 \leqslant Z \leqslant 15$ respectively. However, the error in the actual charge estimates is much larger than that given above. We have taken this error into account in the interpretation of the events.

The emission angles of all the secondary particles were measured with reference to the track due to the heaviest fragmentation particle.

We assumed the direction of the heaviest fragmentation particle to be that of the primary particle. This assumption will introduce some errors in the emission angles of fragmentation α particles and fragmentation protons which cannot be neglected and will be discussed later (§ 4.4). All the measurements were performed in this laboratory.

The group of tracks under the heading n_s in tables 1 and 2, were further separated into subgroups according to their lntan θ distributions.

(i) Isobar process where both incident and target nucleons were in excited states and decay into nucleons (leading particles) and mesons.

(ii) Pionization process (fireball process as it is sometimes called).

(iii) Knock-on process which we attribute to the elastic scattering of nucleons or groups of nucleons in the nucleus.

(iv) Fragmentation process of the incident nucleus.

(v) Evaporation process of the target nucleus.

The Lorentz factors of the primary particles were determined by taking the weighted average (according to the number of tracks in the group) of the several Lorentz factors obtaining by using the $\langle \text{lntan } \theta \rangle$ values for the processes (i)–(iv) in equation (3.2).

3. Estimation of lntan θ distribution

The Lorentz transformation of an angle of a particle in its production system to the laboratory system (LS) is given by:

$$\gamma \tan \theta_s = \frac{\sin \theta_s^*}{(\beta/\beta_s^*) + \cos \theta_s^*} \equiv \alpha_s \tag{3.1}$$

where the subscript 's' denotes secondary particles and the asterisk refers to the emitting rest system. The Lorentz factor γ (velocity β) and the dispersion σ from the lntan θ distribution of the secondaries are obtained from:

$$\gamma = C \exp(-\langle \text{lntan } \theta_s^* \rangle), \qquad C = \exp(\langle \ln \alpha_s \rangle), \tag{3.2}$$

and

$$\sigma^2 = [\langle (\ln \alpha_s)^2 \rangle - (\langle \ln \alpha_s \rangle)^2]/(\ln 10)^2, \tag{3.3}$$

where $\langle \ldots \rangle$ denotes the average taken over β_s^* and $\cos \theta_s^*$ and is given by:

$$\langle (\ln \alpha_s)^n \rangle = \int_0^\infty dp_s^* \int_0^\pi d\theta_s^* F(p_s^*, \theta_s^*) \left(\ln \frac{\sin \theta_s^*}{(\beta/\beta_s^*) + \cos \theta_s^*} \right)^n, \tag{3.4}$$

where $F(p_s^*, \theta_s^*)$ is the momentum and angular distribution function of a group of particles produced through a particular process in its production rest system. Thus, the problem is to know $F(p_s^*, \theta_s^*)$ and the velocity β to obtain $\langle \text{lntan } \theta \rangle$ and σ of specified groups of particles to be described below.

3.1. Fragmentation process

The fragmentation products: protons, P_F; α particles, α_F; and heavier nuclei are those due to the disintegration taking place in an incident nucleus which is excited and is moving in the LS with almost the same velocity as the primary nucleus. The process is well described by the evaporation theory of an excited nucleus. However, the experimental energy and angular distributions in the rest system of the excited nucleus have excess particles in the high-energy region and in the forward direction which cannot be explained by the evaporation theory (Powell *et al* 1959) and are discussed separately (§ 3.2).

Assuming the evaporation theory: an isotropic angular distribution and a Maxwell–Boltzmann energy distribution, and that the potential barrier of the nuclei in our case is zero, the distribution function is given by:

$$F(p^*, \theta^*)\,\mathrm{d}p^*\,\mathrm{d}\theta^* = N \exp(-p^{*2}/2MT_0)p^{*2} \sin\theta^*\,\mathrm{d}p^*\,\mathrm{d}\theta^*, \tag{3.5}$$

where M and p^* are the mass and momentum of the particles in the rest system of the emitting nucleus with temperature T_0. The average value $\langle \mathrm{lgtan}\,\theta\rangle$ and the dispersion σ are calculated in appendix 2 as:

$$E(\mathrm{MB, Iso}) = (4M\langle T\rangle/3e^C)^{1/2}10^{-\langle \mathrm{lgtan}\,\theta\rangle}d, \tag{3.6}$$

and

$$\sigma^2 = (0{\cdot}43)^2[(\pi^2/24)-(T/9M)] \simeq (0{\cdot}279)^2, \tag{3.7}$$

where

$$C = 0{\cdot}5772\ldots, \qquad d = \exp(4\langle T\rangle/3M) \simeq 1,$$

and $\langle T\rangle$ is the average kinetic energy of the fragments in the rest system of the incident nucleus ($T \ll M$).

Since Kaplon's formula (Kaplon *et al* 1952):

$$E(\mathrm{Kaplon}) = (\langle p^2\rangle)^{1/2} = (4M\langle T\rangle/3)^{1/2}10^{-\lg(\langle\theta^2\rangle)^{1/2}} \tag{3.8}$$

is derived assuming mono-energetic and isotropic angular distributions in the emitting rest system, the $\langle \mathrm{lgtan}\,\theta\rangle$ and σ of the particles for the same distributions are calculated in appendix 1 and are given as:

$$E(\mathrm{Mono, Iso}) = (2/e)(2M\langle T\rangle)^{1/2}10^{-\langle \mathrm{lgtan}\,\theta\rangle}, \tag{3.9}$$

and

$$\sigma = (0{\cdot}43)[1-(\pi^2/12)]^{1/2} = 0{\cdot}183. \tag{3.10}$$

The ratios, $E(\mathrm{Mono, Iso}):E(\mathrm{MB, Iso}):E(\mathrm{Kaplon})$ calculated from the equations (3.6), (3.8) and (3.9) give: $1{\cdot}2:1{\cdot}0:1{\cdot}33R$ where $R \equiv \exp\{2{\cdot}3[\langle \mathrm{lgtan}\,\theta\rangle - \lg(\langle\theta^2\rangle)^{1/2}]\}$. The ratio gives $R = 0{\cdot}90$, provided that $E(\mathrm{Kaplon}) = E(\mathrm{Mono, Iso})$. The experimental ratios obtained $E(\mathrm{Mono, Iso}):E(\mathrm{MB, Iso}):E(\mathrm{Kaplon}) = 1{\cdot}12:1{\cdot}0:1{\cdot}26$ give $R = 0{\cdot}95$ for $\alpha_F + P_F$. This value for R is plausible because the RMS average of $\tan\theta$ is never less than the geometric average, ie $\langle \mathrm{lntan}\,\theta\rangle \leqslant \ln(\langle\tan^2\theta\rangle)^{1/2} \simeq \ln(\langle\theta^2\rangle)^{1/2}$. Kaplon's formula and $E(\mathrm{Mono, Iso})$ will give higher values for the primary energy than $E(\mathrm{MB, Iso})$.

The positions on the $\mathrm{lgtan}\,\theta$ plot of groups of the fragmentation α particles and protons as given by (3.6) are centred at

$$\langle \mathrm{lgtan}\,\theta_\alpha\rangle = -\lg\gamma_0 - 1{\cdot}31, \qquad \text{for } \langle E^*_\alpha\rangle = 12\ \mathrm{MeV}, \tag{3.11}$$

$$\langle \mathrm{lgtan}\,\theta_p\rangle = -\lg\gamma_0 - 1{\cdot}01, \qquad \text{for } \langle E^*_p\rangle = 12\ \mathrm{MeV}. \tag{3.12}$$

3.2. Knock-on process

3.2.1. Knock-on protons P_k. The production mechanism of knock-on protons in high-energy nuclear collisions is not clear. Up to the present, the interpretation that knock-on protons and α particles are produced by the intranuclear cascade process was favoured but it predicts little about the angular and energy distributions of the knock-on particles. There is, however, strong support for the interpretation that they are protons elastically

scattered in the collision between primary and target protons in the nucleus (Imaeda *et al* 1971). In this case, the four-momentum transfer distribution is given by

$$N(t)\,\mathrm{d}t = C\exp(Bt)\,\mathrm{d}t \tag{3.13}$$

where B varies only slowly with the primary energy and in the case of protons from elastic π meson–nucleon collisions no change in the four-momentum transfer distribution is reported (Foley *et al* 1963a, b). Then, the kinetic energy distribution of the knock-on protons in the laboratory system is derived from (3.13) and is given by:

$$N(T)\,\mathrm{d}T = C'\exp(-aT)\,dT, \qquad a \equiv 2MB. \tag{3.14}$$

The empirical energy distribution of target knock-on protons in the LS is well represented by the exponential formula (3.14) with $a = 13{\cdot}5\ \mathrm{GeV}^{-1}$.

The empirical angular distribution of the knock-on protons is given by (Imaeda *et al* 1971):

$$f(\theta^*)\,\mathrm{d}\theta^* = \tfrac{5}{18}(5+6\cos\theta^*+8\cos^2\theta^*)\,\mathrm{d}\cos\theta^*. \tag{3.15}$$

The shape of the angular distribution (3.15) depends on the value of B in (3.13). The value of $\langle \mathrm{lgtan}\,\theta\rangle$ for the energy and angular distributions given by (3.14) and (3.15) respectively is derived in appendix 3:

$$\langle \mathrm{lgtan}\,\theta_{\mathrm{kp}}\rangle = -\lg\gamma_0 - 0{\cdot}50. \tag{3.16}$$

The lgtan θ distribution does not have any pronounced maximum.

3.2.2. Knock-on α particles α_{k}. Although little attention has been paid to the knock-on α particles among the fragmentation α particles as mentioned before, there is little doubt that knock-on α particles are present. However, it is difficult to identify these particles unless the expected positions on the lntan θ plot of the knock-on and fragmentation α particles are quite different and are known. As has been discussed in the case of α particles emitted from nuclei at rest in the LS by several authors (Hodgson 1958, Ostroumov and Filov 1960, Baker and Katcoff 1961, Danysz 1962, Poril 1964), the knock-on α particles, denoted by α_{k}, contribute to the forward excess of α particles in their emission angle distribution, and a fraction of the excess forward α particles equal to 0·33 of the total α particles is reported by Hodgson (1958). This forward excess cannot be explained by the motion of the emitting nucleus after the collision. If the forward excess is mainly due to knock-on α particles, at least the fraction 0·33 of the total α particles should be due to the knock-on process. Therefore, the energy and angular distributions of α particles emitted from light (C, N, O) and heavy (Ag, Br) nuclei in emulsion cannot be explained by the evaporation process alone. Their lgtan θ distribution is obtained as follows.

We assume: (i) they have the same kinetic energy distribution as the proton, ie,

$$C'\exp(-2BMT)\,\mathrm{d}T \tag{3.17}$$

where T is the kinetic energy of the α particles. (ii) they have the same momentum distribution as the proton. Then, the value of B in equation (3.17) is given for (i) $B = 3{\cdot}38\ \mathrm{GeV}^{-1}$ and (ii) $B = 13{\cdot}5\ \mathrm{GeV}^{-1}$, respectively. These kinetic energy distributions with the angular distribution (3.15) and energy cut-off, $E \geqslant 30$ MeV, give $\langle \lg\alpha\rangle = -0{\cdot}746$ for (i) and $\langle \lg\alpha\rangle = -0{\cdot}843$ for (ii). The value of $\langle \lg\alpha\rangle$ does not

depend on the value of B to any great extent. We use the mean value $-0{\cdot}79$ for the knock-on α particles and thus, we obtain (appendix 3):

$$\langle \mathrm{lgtan}\,\theta_{\alpha k}\rangle = -\lg\gamma_0 - 0{\cdot}79. \tag{3.18}$$

3.3. Intranuclear cascade process

Besides the composite primary nucleon–nucleon collisions in nucleon–nucleus and nucleus–nucleus collisions, successive collisions of incident nucleons and collisions of produced particles with nucleons in both the incident and target nuclei may take place.

The positions on the lntan θ plot of the secondaries from these processes are spread between the isobar decay mesons and the fragmentation protons of the primary nucleus–nucleus collisions.

3.4. Isobar process

Isobars are emitted in the extreme forward and backward directions as distinct from fireballs which are thought to be produced nearly at rest in the CMS of the colliding nucleons (Imaeda and Kazuno 1963, Kazuno 1964, 1967).

When an isobar decays into a nucleon and one or more mesons, the position on the lgtan θ plot of these secondaries may be predicted if the Lorentz factor $\tilde{\gamma}_{N^*}$ of this isobar in the CMS is known.

3.4.1. Incident isobar decay protons P_I and mesons π_I. For the secondary particles from the decay of an incident isobar having mono-energetic and isotropic angular distributions in the isobar rest system, the average value and dispersion of their lgtan θ distribution are given by (3.9) and (3.10), in which E, M and T should be replaced by those of an isobar. The average values $\langle \mathrm{lgtan}\,\theta\rangle$ of the incident isobar decay proton group denoted by P_I and the meson group denoted by π_I are related by (3.9) to the Lorentz factor of the isobar γ_{N^*}, in the LS as follows:

$$\langle \mathrm{lgtan}\,\theta_p\rangle = -\lg\gamma_{N^*} + \lg\alpha_p = -\lg\gamma_0 - 0{\cdot}03, \tag{3.19}$$

$$\langle \mathrm{lgtan}\,\theta_\pi\rangle = -\lg\gamma_{N^*} + \lg\alpha_\pi = -\lg\gamma_0 + 0{\cdot}35, \tag{3.20}$$

where $\lg\alpha_p$ and $\lg\alpha_\pi$ are given by (A.2) in appendix 1. The separation of the proton and meson groups on the lgtan θ plot is equal to $\lg\alpha_p - \lg\alpha_\pi$ and is greater than the dispersion of the individual groups as given by (3.10) and thus, these groups may be separated experimentally on the lgtan θ plot.

3.4.2. Target isobar decay product T. In contrast with the incident isobars, the separation between the centres of the lgtan θ distributions of the mesons denoted by π_T and the protons denoted by P_T emitted from a target isobar is small and the distributions cannot be separated. The $\langle \mathrm{lgtan}\,\theta\rangle$ for T expected from the experiment is about 0 (Kazuno 1964).

3.5. Fireball process π_{FB}

This process is sometimes called the pionization process. We define fireballs as being produced more or less at rest in the CMS of the colliding nucleons, and the subsequent decay into mesons is denoted by π_{FB}.

Since the transverse momentum of a fireball is small and is less than 3 GeV/c (Imaeda and Fleming 1969), this effect on the angular distribution of the secondaries from a fireball may be neglected. To estimate the $\langle \lg\tan\theta \rangle$ of the secondaries from fireballs (FB), we use the P_t (transverse momentum) distribution of the secondaries which is almost independent of the type and energy of nucleon–nucleon collisions (Cocconi *et al* 1961, Imaeda 1967). Assuming an exponential distribution for the P_t distribution, ie,

$$P_t \exp(-P_t/p_0)\, dP_t, \tag{3.21}$$

where $p_0 = 0{\cdot}14$ GeV/c, the average value of the ltan θ distribution which is independent of the angular distribution used, is given by (Imaeda 1965, Imaeda and Shah 1966):

$$\langle \lg\tan\theta_{FB} \rangle = -\lg\gamma_c - 0{\cdot}1 \simeq -\tfrac{1}{2}\lg\gamma_0 + 0{\cdot}05. \tag{3.22}$$

where

$$\gamma_c = \{(\gamma_0+1)/2\}^{1/2}.$$

The dispersion σ of the lgtan θ distribution of fireball mesons and its primary energy dependence have been studied by Imaeda (1962, 1968a, b).

The experiments have shown that σ for jets of primary energy 100 GeV is nearly isotropic, ie, $\sigma = 0{\cdot}36$ and even if a number of fireballs are emitted they are produced almost at rest in the CMS. Therefore, in our sample, as most of the jets used have primary energy less than 100 GeV/nucleon, σ may be put equal to 0·36.

3.6. Summary of § 3

From the above discussions, we see from (3.11), (3.12), (3.16), (3.18)–(3.20) that the positions on the lgtan θ plot of the average values of the groups: α_F, α_K, P_F, P_K, P_I and π_I, increase with lg γ_0 and their relative positions do not depend on the primary energy. The relative separations of the groups π_{FB} and any of the other groups is proportional to $\frac{1}{2}\lg\gamma_0$ as given by (3.22).

4. Analysis of the experimental ltan θ distribution

We now describe the criteria for separation of the secondaries into the groups mentioned in § 3.

4.1. Heavy ionizing particles

All the heavy ionizing particles are classified into groups: the disintegration products of the target nucleus through the evaporation and knock-on processes, and the fragmentation products ($Z \geqslant 2$) of the incident nucleus. The separation of the particles producing heavily ionizing tracks from the rest can be made reliably by visual inspection. Therefore, we concentrate our effort mainly on the separation of the minimum ionizing particles.

4.2. Minimum ionizing particles

4.2.1. Incident protons P_I. The number N_p of the incident protons is estimated by: (the charge of the primary) − (the sum of the charges of the fragments $Z_f \geqslant 2$).

We assume that particles with emission angles less than or equal to the N_pth smallest-angled minimum ionizing track are due to the incident protons.

4.2.2. Target isobar decay protons P_T. The target isobar decay products P_T constitute a group of N_T largest-angled minimum ionizing tracks which consist of mesons and protons. It is not possible to separate among the target isobar decay products, the protons P_T from the mesons π_T. Therefore, we classify only the target isobar decay products T on the lntan θ plot.

4.3. Created mesons

The protons which produce thin tracks can be further subdivided into the groups P_I, P_F and P_k, the last of which is distributed between the P_I and P_F groups. Therefore, the unique separation of the three groups is not always possible. The expected distance between the centres of the two groups P_I and P_F is 1·27 which is much greater than the sum of their dispersions $\sigma(P_F) = 0{\cdot}28$ and $\sigma(P_k) = 0{\cdot}18$. Using the formulae (3.12), (3.16) and (3.19) for the centres of the three groups and the dispersions $\sigma(P_F)$ and $\sigma(P_k)$, we can separate the groups P_I, P_k and P_F when ln γ_0 is known.

As regards the isobar decay mesons, the unique identification of the mesons from the decay protons is difficult from the lntan θ plot alone. We may assess the multiplicity of the incident (or target) isobar decay mesons n_{π_I} (or n_{π_T}) by subtracting n_{p_I} (or n_{p_T}) from the number of the incident (or target) isobar decay products.

The distances between the expected centres of the following groups: π_I, π_{FB} and π_T, depend on the primary energy and are given by:

$$\text{lgtan } \theta_{\pi_I} - \text{lgtan } \theta_{\pi_{FB}} = \tfrac{1}{2} \lg \gamma_0 - 0{\cdot}41, \tag{4.1}$$

$$\text{lgtan } \theta_{\pi_{FB}} - \text{lgtan } \theta_{\pi_T} = \tfrac{1}{2} \lg \gamma_0 - 0{\cdot}45. \tag{4.2}$$

The dispersions of the groups π_I, π_{FB} and π_T were estimated as 0·32, 0·36 and 0·32, respectively. Fixing the expected value of the lntan θ plot for the groups π_I, π_{FB} and π_T by using the $\langle \text{lntan } \theta \rangle$ positions of the α particle and proton groups given in the above as a guide, we then subdivide the mesons into π_I, π_{FB} and π_T groups by cutting at the minimum track density points (largest gap) on the lntan θ plot between the π_I, π_{FB} and π_T points. This procedure means that the probability that a particle belongs to its assigned group is always greater than 50%.

4.4. Superposition of the lgtan θ plot

To see the validity of the separation method described above, three kinds of superposition of the lgtan θ plots of all the events were produced, taking the following points as the origin of the coordinate of each plot: A, the centre of the incident isobar groups, π_I; B, the centre of the fireball groups, π_{FB}; and C, the origin of the individual lgtan θ plot of all the events.

In superposition A, we can see in figure 1 that the two maxima corresponding to the groups π_I and π_{FB} with the π_I maximum showing a pronounced peak as we would expect. The π_{FB} maximum appears at the position approximately given by the average value of $\langle \frac{1}{2} \lg \gamma_0 \rangle$. A slight bump due to the P_I group appears at 0·38 from the π_I maximum on the lgtan θ plot as expected. A broad tail at the right-hand side of P_I is due to the knock-on P_k, intranuclear cascade P_I and the fragmentation P_F proton groups. The spread of the

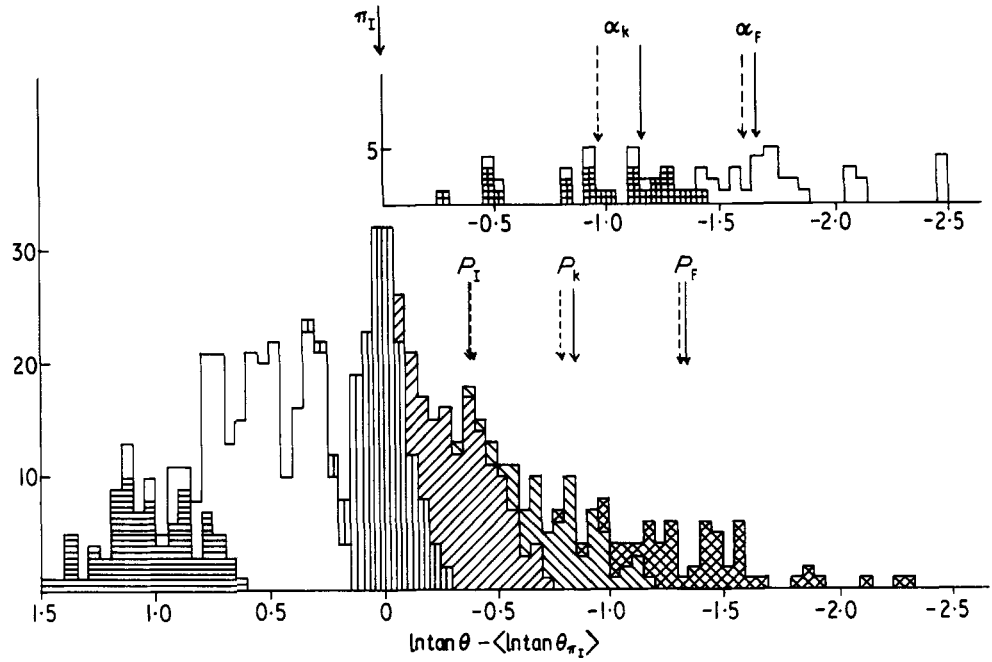

Figure 1. Superposition of the ln tan θ distribution of all the jet taking the centre of the incident isobar meson group as the origin of the coordinate. Full arrows and broken arrows indicate the theoretical and experimental values respectively of $\langle \ln\tan\theta - \langle\ln\tan\theta_{\pi_I}\rangle\rangle$ for the individual groups of secondaries: P_I, P_k, P_F, α_k and α_F. ☐ and ⊞ denote the fragmentation and knock-on α particles, respectively. ⊠, ⧅, ◪, ◫, ☐ and ⊟ denote the fragmentation, knock-on, isobar decay protons, isobar, fireball mesons and target isobar decay particles, respectively.

distribution of all the α particles is much broader and their average lgtan θ value is much larger than that expected from the calculations given in § 3. The reasons may be that: (i) the α particles include those due to the fragmentation and knock-on processes; and (ii) the angles of the α particles with respect to the primary direction include errors due to the uncertainty in defining the primary direction. If the effect of the latter overestimation is taken into account, the average lgtan θ values and dispersions σ of the α particles and the fragmentation protons would be in much better agreement with that expected (see table 3). The spread of the superimposed α particle distribution is due to the inclusion of the knock-on α particles with the fragmentation α particles and the underestimation of

Table 3. Comparison of the experimental values of $\langle\ln\tan\theta\rangle$ and the dispersion σ with those of the theoretical vlues for various groups of secondaries.

	$\langle\lg\tan\theta\rangle_{exp}$	$\langle\lg\tan\theta\rangle_{theor}$	σ_{exp}	σ_{theor}
π_I	$-0{\cdot}005+\lg\gamma_0$	$-0{\cdot}005+\lg\gamma_0$	0·103	0·32
P_I	$-0{\cdot}389+\lg\gamma_0$	$-0{\cdot}385+\lg\gamma_0$	0·165	0·18
P_k	$-0{\cdot}791+\lg\gamma_0$	$-0{\cdot}855+\lg\gamma_0$	0·190	—
P_F	$-1{\cdot}325+\lg\gamma_0$	$-1{\cdot}365+\lg\gamma_0$	0·324	0·279
α_k	$-0{\cdot}963+\lg\gamma_0$	$-1{\cdot}145+\lg\gamma_0$	0·315	—
α_F	$-1{\cdot}615+\lg\gamma_0$	$-1{\cdot}665+\lg\gamma_0$	0·467	0·279

the primary energy resulting from the use of the opening angle of all the α particles is mainly due to the inclusion of these knock-on α particles with the pure fragmentation α particles as well as the error in estimating the primary direction for which the formulae (Kaplon's and equations (3.6), (3.8) and (3.9)) are meant.

After the identification of the various groups of secondaries, the experimental values of $\langle \lg\tan\theta_i - \langle \lg\tan\theta_{\pi_I}\rangle\rangle_A$, the experimental averaged relative distance of the tracks of one of the groups A and its dispersion σ_A have been calculated and are listed in table 3 for the groups π_I, P_I, P_k, P_F, α_k and α_F as well as the theoretical values.

By comparing the second and third columns, we see that the average values for all the groups agree well with the theoretical ones. The experimental values of σ are larger for the α_F and P_F groups but are smaller for the π_I and P_I groups than the corresponding theoretical values. The large experimental values of the σ can be explained as due mainly to the errors in the determination of the direction of the primary, while the smaller values of σ for the groups π_I, P_I and P_k are due to the cut-off procedure in their identification mentioned above.

The superposition B shows only two maxima corresponding to the fireball mesons π_{FB} and the incident isobar decay mesons π_I. The appearance of the maximum due to π_I comes from the fact that the primary energies of the events used do not differ much from each other so that the position of the maximum π_I falls close to the point $-\langle \lg\gamma_0\rangle$.

The superposition C shows two maxima corresponding to π_{FB} and to the incident mesons π_I. The protons from the isobars P_I, knock-on P_k, fragmentation P_F do not manifest any distinct maximum.

5. Results

5.1. Primaries

5.1.1. Dependence on target nucleus. The effects of the nature of the target nucleus on the fragmentation and knock-on particles are given in table 4. There is no substantial difference between the proton target events (PT) and the nucleus target events (NT) in the experimental values of $\langle N_{\alpha_F}\rangle$, $\langle N_{\alpha_k}\rangle$, $\langle N_{P_F}\rangle$, and $\langle N_{P_k}\rangle$ while the values of $\langle N_{P_I}\rangle$, $\langle N_{\pi_I}\rangle$, $\langle N_{\pi_{FB}}\rangle$ and $\langle N_T\rangle$ are larger for the NT events than for the PT events (table 5). The ratios $\langle N_{P_T}(\mathrm{NT})\rangle/\langle N_{P_I}(\mathrm{PT})\rangle$ and $\langle N_T(\mathrm{NT})\rangle/\langle N_{P_I}(\mathrm{PT})\rangle$ suggest that twice as many fireball and isobar mesons are produced in the NT events as in the PT events.

Since our data are collected by area scanning, the bias against events with $N_\alpha + N_f \leqslant 3$ tends to increase the value of $\langle N_{\alpha_F} + N_{\alpha_k}\rangle$. Our value of $\langle N_{\alpha_F} + N_{\alpha_k}\rangle$ gives high values compared to those given by others (Waddington 1960, Judek and van Heerden 1966) which are based on track scanning (table 9).

Table 4. Proton and nucleus target events (primary, fragments and knock-on secondaries)

Subgroup	Number of events	$\langle Z_p\rangle$	$\langle E_p\rangle$ (GeV)	$\langle N_{Z_F\geqslant 3}\rangle$	$\langle Z_F\rangle$	$\langle N_{\alpha_F}\rangle$	$\langle N_{\alpha_k}\rangle$	$\langle N_{P_F}\rangle$	$\langle N_{P_k}\rangle$
Proton target	29	13·5	15·8	0·69±0·15	5·5±0·4	1·21±0·20	0·52±0·14	1·07±0·19	1·31±0·25
Nucleus target	22	14·1	20·0	0·63±0·17	5·0±0·5	0·91±0·20	0·55±0·16	1·64±0·27	1·50±0·26
All	51	13·8	17·9	0·67±0·11	5·3±0·3	1·10±0·14	0·53±0·10	1·31±0·16	1·41±0·17

Table 5. Proton and nucleus target events (the particles from inelastic collisions and target nucleus)

Subgroup	$\langle N_{P_I} \rangle$	$\langle N_{\pi_I} \rangle$	$\langle N_{\pi_{FB}} \rangle$	$\langle n_b \rangle$	$\langle n_g \rangle$	$\langle N_T \rangle$
Proton target	$1{\cdot}97 \pm 0{\cdot}26$	$2{\cdot}07 \pm 0{\cdot}27$	$3{\cdot}00 \pm 0{\cdot}32$	$0{\cdot}21 \pm 0{\cdot}09$	$0{\cdot}24 \pm 0{\cdot}09$	$1{\cdot}17 \pm 0{\cdot}20$
Nucleus target	$3{\cdot}50 \pm 0{\cdot}40$	$4{\cdot}95 \pm 0{\cdot}46$	$7{\cdot}00 \pm 0{\cdot}56$	$2{\cdot}27 \pm 0{\cdot}32$	$1{\cdot}73 \pm 0{\cdot}28$	$3{\cdot}54 \pm 0{\cdot}40$
All	$2{\cdot}43 \pm 0{\cdot}22$	$3{\cdot}15 \pm 0{\cdot}28$	$4{\cdot}73 \pm 0{\cdot}30$	$1{\cdot}10 \pm 0{\cdot}14$	$0{\cdot}88 \pm 0{\cdot}13$	$2{\cdot}18 \pm 0{\cdot}20$

Table 6. High- and low-energy events (primary, fragments and knock-on secondaries)

Subgroup	Number of events	$\langle Z_p \rangle$	$\langle E_p \rangle$ (GeV)	$\langle N_{Z_F \geqslant 3} \rangle$	$\langle Z_F \rangle$	$\langle N_{\alpha_F} \rangle$	$\langle N_{\alpha_k} \rangle$	$\langle N_{P_F} \rangle$	$\langle N_{P_k} \rangle$
High-energy	27	12·4	28·3	$0{\cdot}59 \pm 0{\cdot}15$	$4{\cdot}4 \pm 0{\cdot}4$	$1{\cdot}04 \pm 0{\cdot}19$	$0{\cdot}52 \pm 0{\cdot}14$	$1{\cdot}47 \pm 0{\cdot}24$	$1{\cdot}48 \pm 0{\cdot}23$
Low-energy	24	14·4	9·5	$0{\cdot}75 \pm 0{\cdot}18$	$6{\cdot}2 \pm 0{\cdot}5$	$1{\cdot}17 \pm 0{\cdot}22$	$0{\cdot}54 \pm 0{\cdot}15$	$1{\cdot}25 \pm 0{\cdot}23$	$1{\cdot}33 \pm 0{\cdot}24$

5.1.2. Primary energy dependence. The values of $\langle N_{\alpha_F} \rangle$, $\langle N_{Z_f \geqslant 3} \rangle$ and $\langle N_{\alpha_k} \rangle$ for the high-energy (HE) group and the low-energy (LE) group shows that they do not depend on the primary energy. The result agrees with Waddington (1960).

The quantities $\langle N_{P_I} \rangle$, $\langle N_{\pi_I} \rangle$, $\langle N_{\pi_{FB}} \rangle$ and $\langle N_T \rangle$ reveal marked increases with the primary energy (table 7).

5.1.3. Primary charge dependence. The main difference in the features of two groups, the heavier ($13 \leqslant Z \leqslant 26$) primary events (HP) and the lighter ($6 \leqslant Z \leqslant 12$) primary events (LP), is that the average charge $\langle Z \rangle$ carried away by the fragments ($Z \geqslant 3$) for the HP jets is much larger than for the LP jets as shown in table 8. The number of α particles per event is nearly equal in both cases. There is a tendency for the numbers of α_k, P_k, P_I, π_I and π_{FB} to be larger for the HP events than for the LP events.

Table 7. High- and low-energy events (the particles from inelastic collisions and target nucleus)

Subgroup	$\langle N_{P_I} \rangle$	$\langle N_{\pi_I} \rangle$	$\langle N_{\pi_{FB}} \rangle$	$\langle n_b \rangle$	$\langle n_g \rangle$	$\langle N_T \rangle$
High-energy	$3{\cdot}04 \pm 0{\cdot}34$	$4{\cdot}33 \pm 0{\cdot}27$	$7{\cdot}30 \pm 0{\cdot}52$	$1{\cdot}37 \pm 0{\cdot}23$	$1{\cdot}11 \pm 0{\cdot}20$	$3{\cdot}15 \pm 0{\cdot}34$
Low-energy	$2{\cdot}17 \pm 0{\cdot}30$	$1{\cdot}83 \pm 0{\cdot}28$	$1{\cdot}83 \pm 0{\cdot}28$	$0{\cdot}83 \pm 0{\cdot}19$	$0{\cdot}63 \pm 0{\cdot}16$	$1{\cdot}08 \pm 0{\cdot}21$

Table 8. Heavier and lighter primary events (primary, fragments and knock-on secondaries)

Subgroup	Number of events	$\langle Z_p \rangle$	$\langle E_p \rangle$ (GeV)	$\langle N_{Z_f \geqslant 3} \rangle$	$\langle Z_F \rangle$	$\langle N_{\alpha_F} \rangle$	$\langle N_{\alpha_k} \rangle$	$\langle N_{P_F} \rangle$	$\langle N_{P_k} \rangle$
Heavier primary	27	17·8	18·7	$0{\cdot}93 \pm 0{\cdot}19$	$8{\cdot}6 \pm 0{\cdot}6$	$0{\cdot}95 \pm 0{\cdot}19$	$0{\cdot}63 \pm 0{\cdot}15$	$1{\cdot}37 + 0{\cdot}23$	$1{\cdot}48 \pm 0{\cdot}23$
Lighter primary	24	9·2	16·7	$0{\cdot}38 \pm 0{\cdot}13$	$1{\cdot}5 \pm 0{\cdot}3$	$1{\cdot}25 \pm 0{\cdot}23$	$0{\cdot}42 \pm 0{\cdot}13$	$1{\cdot}25 \pm 0{\cdot}23$	$1{\cdot}00 \pm 0{\cdot}20$

5.2. Secondaries

5.2.1. Frequency of particles of charge $Z_f > 2$. The average number of fragments of $Z \geqslant 3$ increases with the charge of the primary nuclei (table 8) but the number of fragmentation α particles does not. The numbers of fragments and α particles show little dependence on the primary energy (table 6). This result supports the result of Waddington (1960) of the non-dependence of the fragmentation parameters on the primary energy. These results also agree with the observations on the number of evaporation black prongs from proton–nucleus interactions which stay constant for primary energies greater than about 10 GeV (Cleghorn *et al* 1968).

Table 9. Fragmentation products of the primary particles ($Z \simeq 10$–26)

Fragmentation products	Present experiment	Judek and van Heerden (1966)	Waddington (1960)
α particles	$1{\cdot}67 \pm 0{\cdot}21$	$1{\cdot}20 \pm 0{\cdot}11$	$1{\cdot}30 \pm 0{\cdot}09$
Light nuclei ($Z \simeq 3$–5)	$0{\cdot}26 \pm 0{\cdot}04$	$0{\cdot}25 \pm 0{\cdot}05$	$0{\cdot}14 \pm 0{\cdot}03$
Medium nuclei ($Z \simeq 6$–9)	$0{\cdot}41 \pm 0{\cdot}10$	$0{\cdot}24 \pm 0{\cdot}08$	$0{\cdot}33 \pm 0{\cdot}04$
Heavy nuclei I ($Z \simeq 10$–19)	$0{\cdot}21 \pm 0{\cdot}07$	$0{\cdot}27 \pm 0{\cdot}05$	$0{\cdot}28 \pm 0{\cdot}05$
Heavy nuclei II ($Z \simeq 20$–26)	$0{\cdot}21 \pm 0{\cdot}07$	$0{\cdot}32 \pm 0{\cdot}06$	$0{\cdot}31 \pm 0{\cdot}04$

5.2.2. Frequency of knock-on α *particles.* A fraction of about 30% of the knock-on α particles exists among the relativistic α particles $\langle N_{\alpha_K} + N_{\alpha_F} \rangle$ (table 4). Although there are no data to compare directly with our result on the knock-on α particles from nucleus targets in the charge region $6 \leqslant Z \leqslant 26$, the result agrees qualitatively with those of Hodgson (1958), Ostroumov *et al* (1960) and Baker and Katcoff (1961) for Ag and Br target nuclei if the forward–backward ratio is higher for lighter target nuclei than for heavier nuclei as we would expect. A similar observation on the emission of heavy fragments of $E_f \geqslant 20$ MeV has been reported by Danysz (1962).

5.2.3. Frequency of knock-on protons. The number of knock-on protons emitted from the target nucleus is $0{\cdot}88 \pm 0{\cdot}13$ per event for all the jets (table 5).

5.2.4. Primary energy estimation by knock-on α *particles and protons.* The knock-on α particles among the fragmentation α particles cause an underestimation for the primary energy if Kaplon's and our formulae (equation (3.6) and (3.8)) for fragmentation α particles are applied for all the relativistic α particles. The underestimation factor for the α particles is 3·3 for α particles (table 3).

A similar case was reported by Rybicki (1967) on the knock-on protons emitted from target nuclei—he showed that the angle of these protons in the anti-laboratory system is larger than that predicted by Kaplon's formula for evaporation protons. He concluded that the average angle in the anti-laboratory system of those nonevaporation protons is four times greater than that predicted by Kaplon's formula, though he did not give a lower limit for their energy nor the proportion of such protons among evaporation protons. However, his value is a little larger than that given by our formula for the knock-on protons.

5.2.5. Frequency of incident isobar protons. We find the average number of inelastic nucleon–nucleon collisions to be $2{\cdot}4 \pm 0{\cdot}4$ in a nucleus–nucleus collision. The result shows that $\langle N_{P_I} \rangle$ is greater for the heavier incident nucleus group ($3{\cdot}2 \pm 0{\cdot}3$) than for the lighter one ($2{\cdot}0 \pm 0{\cdot}3$). Also $\langle N_{P_I} \rangle$ is greater for the nucleus target events than for the proton target events (table 5).

5.2.6. Frequency of isobar mesons. The number of isobar decay mesons per nucleus–nucleus and nucleon–nucleus collision is proportional to that of $\langle N_{P_I} \rangle$ and therefore increases with the primary energy (table 7) and with the charges of primary and target nuclei (table 5).

5.2.7. Frequency of target isobar decay products. $\langle N_T \rangle$ increases with the primary energy (table 7) and is higher for the light nucleus target events than for the proton events (table 5) but shows no significant difference between the heavier primary ($Z \geqslant 13$) and the lighter primary events ($Z < 13$): $\langle N_T \rangle = 2{\cdot}1 \pm 0{\cdot}3$ and $2{\cdot}3 \pm 0{\cdot}3$ respectively. This feature can be explained by isobar production through the nuclear cascade process in the nucleus.

6. Conclusion

The lgtan θ distribution method developed in this paper enables one to separate groups of secondaries, mesons and nucleons from different processes, ie, fragmentation, knock-on, isobar decay and fireball processes, which are produced in primary nucleon–nucleon collisions and in the intranuclear cascade process due to nucleon–nucleon collisions and meson–nucleon collisions in the nucleus. Thus, this knowledge will shed light on the mechanism of particle production in nucleus–nucleus collisions, on extensive air showers due to heavy cosmic rays, and on the production of photons and electrons in in interstellar space.

Acknowledgments

The authors are grateful for the critical and valuable comments of the referees.

Appendix. The average value and the dispersion σ of the ln tan θ distribution of secondary particles

A.1. Isotropic angular and mono-energetic distributions

The function $F(p^*, \theta^*)$ in (3.4) is

$$F(p^*, \theta^*) = \delta(p_0^* - p^*) \sin \theta^*. \tag{A.1}$$

Case (*i*): $m \equiv \beta/\beta^* > 1$. The integration of (3.4) by p^* and θ^* for $n = 1$ is given by Castagnoli *et al* (1953); we find:

$$\langle \ln \alpha \rangle \simeq \ln(2p^*/eE^*\beta), \tag{A.2}$$

and we obtain from (A.2):

$$E = (2/e\beta)(2\langle T\rangle M)^{1/2}10^{-\langle \lg\tan\theta\rangle}. \tag{A.3}$$

The dispersion σ of the $\lg\tan\theta$ distribution for π mesons from the incident isobars is given by 0·39.

For large values of m, the integration of (3.4) for $n = 2$ yields:

$$(2.3\sigma)^2 = 1-\frac{\pi^2}{12}+\frac{2}{75}\frac{1}{m^2}+\frac{4}{225}\frac{1}{m^4}+\ldots. \tag{A.4}$$

Case (ii): $m \equiv \beta/\beta^* \gtrless 1$. Replacing the lower limit of the integral in (3.4) from $\cos\theta^* = -1$ to $-(\beta_N^*/\beta_P^*)$ and using the mono-energetic and $\cos^{2k}\theta^*$ distributions for $F(p^*, \theta^*)$, we obtain for $\langle\ln\alpha\rangle$ by integrating equation (5.4):

$$\langle\ln\alpha\rangle = \frac{1}{1+m^{2\beta+1}}\left(\ln 2-\frac{1}{2}\ln(1-m^2)-\frac{m^{2k+1}}{2}\ln\left(\frac{1+m}{1-m}\right)-\sum_{r=0}^{k}\frac{1+m^{2r+1}}{2r+1}\right.$$
$$\left.+\sum_{r=0}^{2k}\frac{(-m)^r}{2k-r+1}+m^{2k+1}\sum_{r=0}^{2k}\frac{1}{r+1}\right). \tag{A.5}$$

For target protons $m \gtrsim 1$, $\langle\lg\alpha\rangle \simeq 0$. For target isobar decay mesons ($m \simeq 0{\cdot}78$–$0{\cdot}90$) we obtain $\langle\lg\alpha\rangle \simeq 0{\cdot}04$–$0{\cdot}09$.

A.2. Maxwell–Boltzmann energy distribution with isotropic emission

Change the integration variable p^* in (3.5) to $y \equiv p^{*2}/2MT_0$. Expand $\ln\alpha$ of (3.4) in power series of $\beta^*/\beta = axy^{1/2}(1+by)^{-1/2}$, where $a \equiv (2T_0/M)^{1/2}\beta^{-1}$, $b \equiv 2T_0M^{-1}$, $x \equiv \cos\theta^*$, and integrate with respect to y and $\cos\theta^*$. We find (KE = kinetic energy):

$$\exp(\langle\ln\alpha\rangle) = \left(\frac{4\langle T_0\rangle}{3M\beta^2e^C}\right)^{1/2}e^{\delta}, \qquad C = 0{\cdot}577\ldots,$$
$$\delta = -\tfrac{5}{3}\langle\mathrm{KE}\rangle M^{-1}+\mathrm{O}(\langle\mathrm{KE}\rangle^2M^{-2}) \simeq -10^{-2}. \tag{A.6}$$

For σ:

$$(2{\cdot}7\sigma)^2 = \frac{\pi^2}{24}-\frac{1}{9}\langle\mathrm{KE}\rangle M^{-1}+\ldots \simeq \frac{\pi^2}{24}. \tag{A.7}$$

A.3. Exponential four-momentum distribution with anisotropic angular distribution

The average value of $\langle\ln\alpha\rangle$ over $\cos\theta^*$ with the angular distribution

$$(n+1)2\cos^n\theta^*\,\mathrm{d}\cos\theta^*$$

was calculated as:

$$\langle\ln\alpha\rangle = \ln 2+\ln(\beta^*/\beta)-\sum_{t=0}^{k}(2t+1)^{-1}+\sum_{t=0}^{\infty}B_{k,t}(\beta^*/\beta)^{2t+2}, \qquad \text{for even } n = 2k$$
$$B_{k,t} = (2t+2)^{-1}-(2t+2k+3)^{-1},$$

and

$$\langle\ln\alpha\rangle = \sum_{t=0}^{\infty}D_{k,t}(\beta^*/\beta)^{2t+1}, \qquad \text{for odd } n = 2k+1$$
$$D_{k,t} = (2t+1)^{-1}-(2t+2k+3)^{-1}. \tag{A.9}$$

For the lower limit corresponding to $T = 30\,\text{MeV}$ and for $2BM = 13{\cdot}5\,\text{GeV}^{-1}$, we find from (A.8), (A.9) and (3.15):

$$\langle \lg\tan\theta\rangle \begin{cases} = -\lg\gamma_0 - 0{\cdot}50, & \text{for protons,} \\ = -\lg\gamma_0 - 0{\cdot}746, & \text{for } \alpha \text{ particles of } B = 3{\cdot}38\,\text{GeV}^{-1} \\ = -\lg\gamma_0 - 0{\cdot}843, & \text{for } \alpha \text{ particles of } B = 13{\cdot}5\,\text{GeV}^{-1}. \end{cases} \tag{A.10}$$

References

Baker E W and Katcoff B 1961 *Phys. Rev.* **123** 641–6
Castagnoli C, Cortini C, Franzinetti C, Manfredini A and Moreno D 1953 *Nuovo Cim.* **10** 1539–58
Cleghorn T F, Freier P and Waddington C T 1968 *Can. J. Phys.* **46** 572–7
Cocconi G, Koester L J and Perkins D H 1961 UCID-10022 167
Danysz J A 1962 *Polish Acad. Scie. Inst. Nucl. Research Report No* 328/VI, Warsaw
Forley K J *et al* 1963a *Phys. Rev. Lett.* **10** 376, 543
—— 1963b *Phys. Rev. Lett.* **11** 425
Hodgson P E 1958 *Nucl. Phys.* **8** 1–12
ICEF Collaboration 1963 *Suppl. Nuovo Cim.* **1** 1039–90
Imaeda K 1962 *Nuovo Cim.* **26** 417–39
—— 1965 *Nuovo Cim.* **36** 1376–9
—— 1967 *Nuovo Cim.* **48** 482–505
—— 1968a *Nuovo Cim.* A **55** 100–9
—— 1968b *Can. J. Phys.* **46** 722–6
Imaeda K and Fleming P 1969 *Nuovo Cim.* A **62** 439–48
Imaeda K and Kazuno M 1963 *Suppl. Nuovo Cim.* **1** 1197–225
Imaeda K, Kazuno M and Fleming P 1971 *Lett. Nuovo Cim.* **1** 596–600
Imaeda K and Shah T P 1966 *Nuovo Cim.* **41** 405–16
Judek B and van Heerden I J 1966 *Can. J. Phys.* **44** 1121–45
Kaplon M F, Peters B, Reynolds H L and Ritson D M 1952 *Phys. Rev.* **85** 295–309
Kazuno M 1964 *Nuovo Cim.* **34** 303–16
—— 1967 *Nuovo Cim.* **47** 73–84
Ostroumov V I and Filov R A 1960 *Sov. Phys.–JETP* **37** 495
Porile N T 1964 *Phys. Rev.* **135** B371–7
Powell C F, Fowler P H and Perkins D H 1959 *Study of Elementary Particles by the Photographic Method* (Oxford: Pergamon) pp 450–71
Rajopokhye V Y and Waddington C J 1958 *Phil. Mag.* **3** 25
Rybicki K 1967 *Nuovo Cim.* B **49** 203
Waddington C J 1960 *Prog. Nucl. Phys.* **8** 1–45